DOI: 10.1002/chem.200903413

VIP

Confinement Effect of Organic Nanotubes Toward Green Fluorescent Protein (GFP) Depending on the Inner Diameter Size

Naohiro Kameta,*[a, b] Hiroyuki Minamikawa,[a, b] Yuu Someya,[c] Hiroharu Yui,[b, c] Mitsutoshi Masuda,[a, b] and Toshimi Shimizu*[a, b]

Abstract: Transportation, release behavior, and stability of a green fluorescent protein (GFP, 3×4 nm) in self-assembled organic nanotubes with three different inner diameters (10, 20, and 80 nm) have been studied in terms of novel nanocontainers. Selective immobilization of a fluorescent acceptor dye on the inner surface enabled us to not only visualize the transportation of GFP in the nanochannels but to also detect release of the encapsulated GFP to the bulk solution in real time, based on fluorescence resonance energy transfer (FRET). Obtained diffusion constants and release rates of GFP markedly decreased as the inner diameter of the nanotubes was decreased. An *endo*-sensing procedure also clarified the dependence of the thermal and chemical stabilities of the GFP on the inner diameters. The GFP encapsulated in the 10 nm nanochannel showed strong resistance to heat and to a denaturant. On the other hand, the 20 nm nanochannel accelerated the denaturation of the encapsulated GFP compared with the rate of denaturation of the free GFP in bulk and the encapsulated GFP in the 80 nm nanochannels. The confinement effect based on rational fitting of the inner diameter to the size of GFP allowed us to store it stably and without denaturation under high temperatures and high denaturant concentrations.

Keywords: nanotubes · proteins · self-assembly · supramolecular chemistry

Introduction

Supramolecular chemistry has allowed us to produce tubular nanoarchitectures with well-defined size dimensions.[1] Organic nanotubes self-assembled from amphiphilic molecules have hydrophilic channels with inner diameters of between 10 and 100 nm. Therefore, they can act as mesoscale hosts in water. In fact, organic nanotubes are not only able to encapsulate various nanomaterials and biomacromolecules into the nanochannels but also to release those guests to external bulk media.[2,3,4] These functions of the organic nanotubes will lead to useful containers and carriers for new types of drug-delivery systems. We have performed systematic and quantitative studies on the encapsulation/release behavior and release rate of the guests (Table 1), and reported that an electrostatic attraction between the inner surface of the organic nanotubes and the guests is a critical factor in the encapsulation process,[5] whereas weakening of this interaction promotes release.[6] Bellamkonda et al. suggested that the release rate of the encapsulated proteins in the phospholipid nanotube channel depends on their molecular weight or size, namely, the larger proteins are released over a longer period.[7] Fang et al. found that the mobility of the guests in the lipid nanotube channel depends not only on

[a] Dr. N. Kameta, Dr. H. Minamikawa, Dr. M. Masuda, Dr. T. Shimizu
Nanotube Research Center (NTRC)
National Institute of Advanced Industrial Science and Technology (AIST)
Tsukuba Central 5
1-1-1 Higashi
Tsukuba, Ibaraki, 305-8565 (Japan)
Fax: (+81) 29-861-4545
E-mail: n-kameta@aist.go.jp
tshmz-shimizu@aist.go.jp

[b] Dr. N. Kameta, Dr. H. Minamikawa, Dr. H. Yui, Dr. M. Masuda, Dr. T. Shimizu
SORST (Japan) Science and Technology Agency (JST)
Tsukuba Central 5
1-1-1 Higashi
Tsukuba, Ibaraki, 305-8565 (Japan)

[c] Dr. Y. Someya, Dr. H. Yui
Department of Chemistry, Faculty of Science
Tokyo University of Science
Funagawara-machi 12
Ichigaya, Shinjyuku-ku
Tokyo, 162-0826 (Japan)

Supporting information for this article is available on the WWW under http://dx.doi.org/10.1002/chem.200903413.

 © 2010 Wiley-VCH Verlag GmbH & Co. KGaA, Weinheim WILEY InterScience DISCOVER SOMETHING GREAT

Table 1. Comparison of our previous works with this work in terms of organic nanotubes as nanocontainers.[a]

Organic nanotube			Guest	Encapsulation	Release	Dynamic behavior		Stability	
Bolaamphiphile	i.d. [nm]	Probe				Transport	Diffusion	Thermal	Chemical
1	80		nanobeads, ferritin	Ref. [5]					
1	80	Nbd	ds-DNA, QSY-ferritin	Ref. [9]		Ref. [9]	Ref. [9]		
1	80	Alexa	GFP	this work	this work	this work	this work	this work	this work
1	20		ds-DNA, ferritin	Ref. [9]					
1	20	Alexa	GFP	this work	this work	this work	this work	this work	this work
2	7–9		oligo-DNA, CF	Ref. [6]	Ref. [6]				
2	10	Alexa	GFP	Ref. [10]	Ref. [10]	Ref. [10]		Ref. [10]	
3	10		GFP, Mb	Ref. [11]	Ref. [11]				Ref. [11]
3	10	Alexa	GFP	this work	this work	this work	this work	this work	this work

[a] Abbreviations: Nbd = 7-nitrobenzofurazan; Alexa = Alexa Fluor 546 (Molecular Probes); QSY = QSY7 (Molecular Probes); ds-DNA = double-strand DNA (T4GT7-DNA, 166 kbp); oligo-DNA = oligoadenylic acid (40-mer); CF = carboxy fluorescein; Mb = myoglobin.

their positions in the nanochannels but also their respective concentrations.[8] Recently, we also showed that the diffusion[9] and stabilities[10,11] of an encapsulated iron-storage protein (ferritin) and green fluorescent protein (GFP) in the organic nanotube channel are remarkably different from those of free ferritin and GFP in the bulk solvent (Table 1). However, the channel size effect of the organic nanotubes themselves toward such specific phenomena in the one-dimensional nanospace has never been investigated, although it is very important for the stable storage and controlled release of biomacromolecules.

Herein, we describe for the first time the dynamic behavior of GFP, such as transportation and diffusion, release, and stability, in organic nanotube channels with three different inner diameters (this work in Table 1). To directly detect GFP in the nanochannels in real time, we employed an *endo*-sensing procedure based on fluorescence resonance energy transfer (FRET) between GFP and the interior fluorescence acceptor immobilized on the nanotube inner surface. We revealed that the diffusion constant, release rate, and thermal and chemical stabilities of GFP strongly depend on the inner diameters of the organic nanotubes.

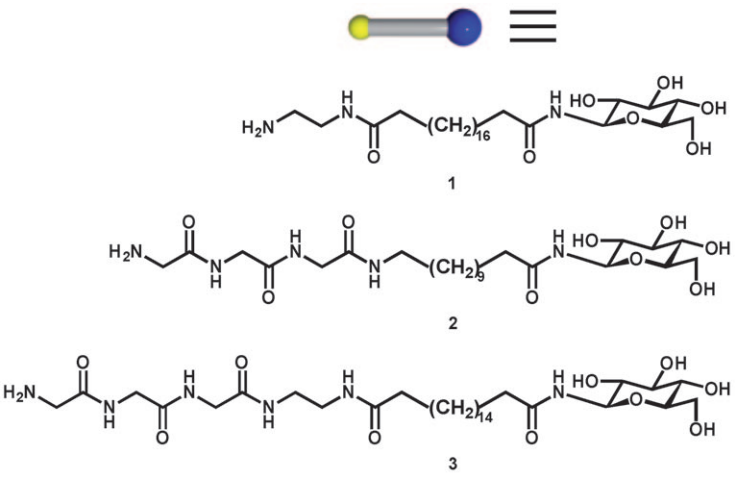

Scheme 1. Asymmetric bolaamphiphiles.

Results and Discussion

Organic nanotubes with 20 and 80 nm inner diameters were prepared by self-assembly of *N*-(2-aminoethyl)-*N*′-(β-D-glucopyranosyl)icosanediamide **1** (Scheme 1) under different pH conditions according to a previous method.[9] An organic nanotube with an inner diameter of 10 nm was prepared by self-assembly of *N*-(β-D-glucopyranosyl)-*N*′-(2-glycylglycylglycineamideethyl)octadecane diamide **3** (Scheme 1) as reported previously.[11] Because the 10 nm organic nanotube self-assembled from *N*-{(11-[(β-D-glucopyranosyl)carbamoyl]undecanyl)}glycylglycylglycine amide **2** had a relatively low gel-to-liquid crystalline phase transition temperature (60 °C),[6,10] the nanotube was unsuitable for the present study, which was often carried out under high temperature conditions. Packing analysis has already shown that all organic nanotubes consist of monolayer lipid membrane in which the amphiphilic molecules pack in a parallel fashion. Therefore, all organic nanotubes have different inner and outer surfaces covered with amino and glucose headgroups, respectively. Alexa Fluor 546 (abbreviated to Alexa; Molecular Probes), which is an optical sensing probe for GFP, was covalently linked to the amino groups on the inner surface of the organic nanotubes (see the Experimental Section). Thus, we obtained Alexa-immobilized nanotubes with inner diameters of 10, 20, and 80 nm (abbreviated hereafter as 10-AlexaNT, 20-AlexaNT, and 80-AlexaNT, respectively). When GFP approaches to within a few nanometers of the Alexa on the inner surface of the nanochannels, Alexa acts as a fluorescence acceptor and GFP acts as a fluorescence donor in a fluorescence resonance energy transfer (FRET).[10] Transmission electron microscopic (TEM) observation revealed that morphological changes and destruction of the tubular structures do not occur after chemical modification (Figure 1). Fluorescence microscopy clearly visualized the 10-, 20-, and 80-AlexaNTs, proving that Alexa was dispersed on the inner surface in the membrane wall over the range of the visualized length (see below).

Diffusion of GFP in organic nanotube channels: Time-lapse fluorescence microscopy observations enabled us to visualize encapsulation and transportation of GFP in the Alexa-functionalized NTs. To efficiently detect FRET from GFP

 © 2010 Wiley-VCH Verlag GmbH & Co. KGaA, Weinheim

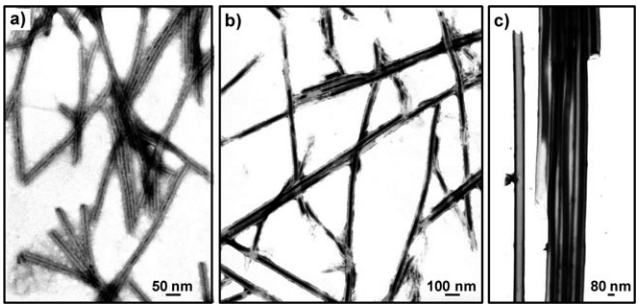

Figure 1. TEM images of a) 10-AlexaNT, b) 20-AlexaNT, and c) 80-AlexaNT that have been negatively stained with phosphotungstate. The hollow cylinder space of the nanotubes can be visualized as the relatively darker area compared with the surroundings.

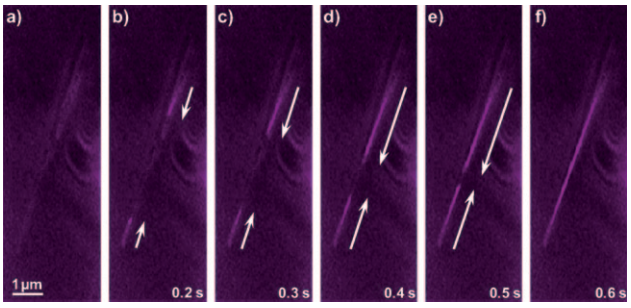

Figure 2. Time-lapse fluorescence microscopic images of 20-AlexaNT upon addition of GFP. The elapsed time is indicated at the bottom of each image. The bands of the excitation and absorption filters are $\lambda =$ 470–495 and 570–625 nm, respectively.

to Alexa, we incorporated excitation ($\lambda = 470$–490 nm) and absorption ($\lambda = 570$–625 nm) filters into a mirror unit to cut the fluorescence of GFP in the bulk solution and suppress the direct excitation of Alexa. Upon addition of GFP at pH 6.8, each open end of the 20-AlexaNT started to be visible and the two bright lines finally reached the center as time elapsed (Figure 2). This phenomenon is ascribable to FRET, in which GFP penetrates the 20-AlexaNT from both ends and gradually excites the Alexa on the inner surface as it flows through the nanochannel (Figure 3). Similar time-lapse images based on FRET were observed in combinations of 10-AlexaNT or 80-AlexaNT with GFP (see the Supporting Information).

The analysis of the obtained time-lapse images demonstrated that a diffusion phenomenon can simulate this transportation feature of GFP well. The square of the migration distance (X^2) of GFP was plotted against the time required for migration (Figure 4). Each obtained linear plot is clearly compatible with the diffusion process. In the present systems, GFP exists in high concentrations in the external solution and diffuses from the open ends of the organic nanotubes ($X = 0$) to the center of the nanochannel ($X > 0$). Therefore, we can apply the equation $[X^2] = 4D\Delta t$ to this system, in which D is a diffusion constant.[12] On the basis of the slope of the linear relationship, we calculated the diffusion constant D of GFP in the nanochannels. The D values are smaller than that of free GFP in bulk (Table 2), which was independently determined by dynamic light scattering (see the Supporting Information). This depression of the diffusion was also observed for the spherical protein ferritin (15 nm) in an 80 nm organic nanotube,[9] and 30 nm latex beads in a fluid-state lipid nanotube (100 nm inner diameter) composed of phospholipids[13] (Table 2).

Furthermore, the D values of GFP decreased remarkably as the inner diameters of the organic nanotubes were decreased (Table 2), which is compatible with a theory that shows a strong reduction in diffusion in restricted nanospaces.[14] According to a pore and surface diffusion model, the apparent diffusion is composed of a pore diffusion on desorption process and a surface diffusion on adsorption pro-

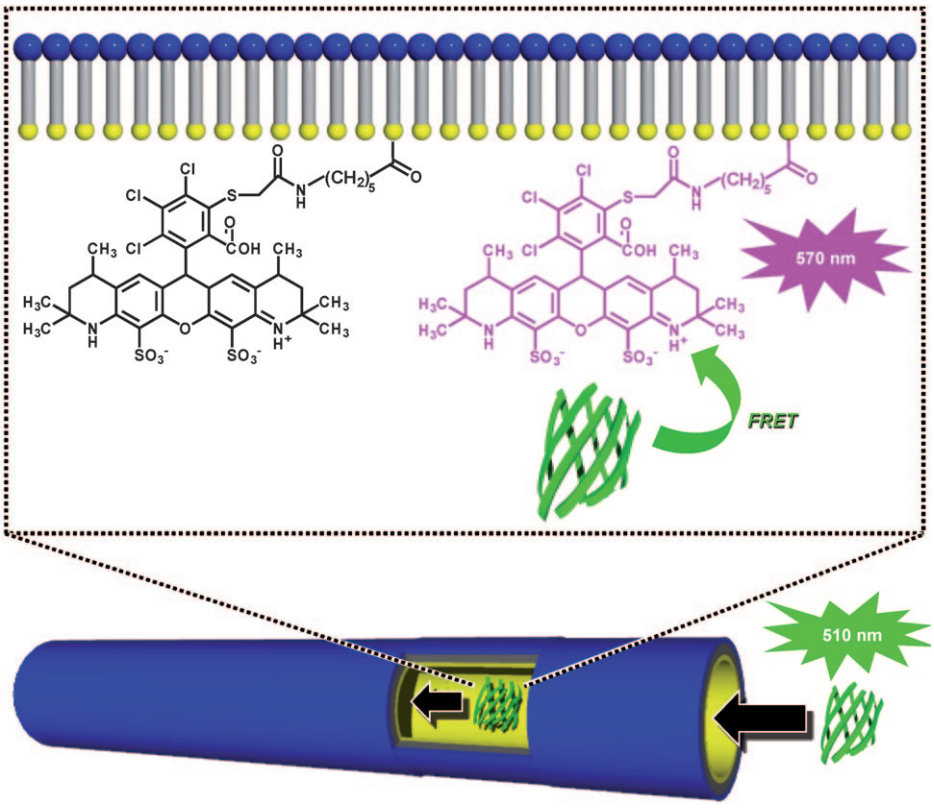

Figure 3. Optical *endo*-sensing of the AlexaNT toward the transportation of GFP by FRET.

© 2010 Wiley-VCH Verlag GmbH & Co. KGaA, Weinheim

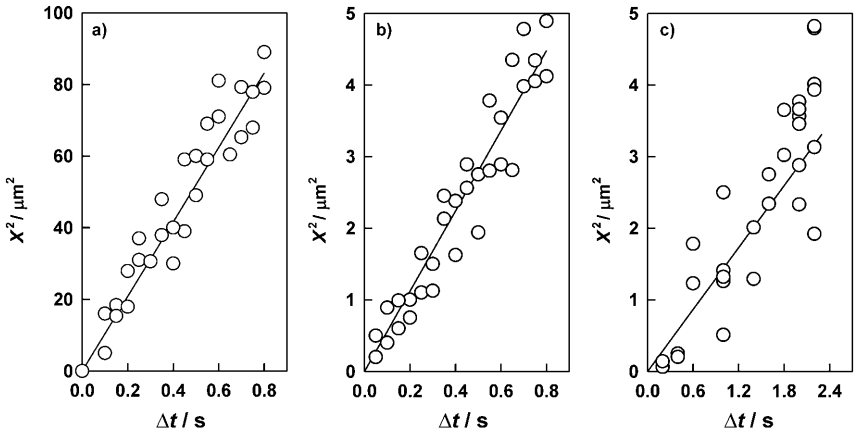

Figure 4. Relationship between the square of the migration distance (X^2) of GFP and the time (Δt) required for migration in a) 80-AlexaNT, b) 20-AlexaNT, and c) 10-AlexaNT.

Table 2. Diffusion constants of various guests in the nanotube channels and the bulk.

Space	Guest (size [nm])	D [10^{-10} m^2 s^{-1}]
bulk	GFP (3–4)	1.2
80-AlexaNT	GFP (3–4)	0.26
20-AlexaNT	GFP (3–4)	0.014
10-AlexaNT	GFP (3–4)	0.0036
bulk	QSY-ferritin (15)	0.34[a]
80 nm NbdNT	QSY-ferritin (15)	0.070[a]
bulk	latex beads (30)	0.20[b]
100 nm NT	latex beads (30)	0.09[b]

[a] Ref. [9]. [b] Ref. [13].

cess.[15] We should also consider a contribution from the electrostatic attraction between the cationic inner surface with protonated amino groups[9,11] and the anionic GFP (isoelectric point pI = 4.7–5.1; ζ-potential −21 mV; see Supporting Information) at pH 6.8, in addition to the physical adsorption.[16] However, the dependence on the inner diameter of the GFP diffusion in the present system is consistent with the model supported by some experimental studies, in which the pore diffusion of dye molecules in silica gels is depressed as the pore sizes are decreased.[17]

Release rate of GFP from the organic nanotube channels to the bulk solution: The release behavior of the encapsulated GFP in the organic nanotube channels was monitored by using this FRET system. Free GFP in the bulk solution was removed before monitoring. The fluorescence spectra that represent the FRET from the encapsulated GFP to the interior Alexa hardly changed, even after 80 h at pH 6.8 (Figure 5, top). This result indicates that the encapsulated GFP stays in the nanochannel (Figures 3 and 6). The cationic inner surface of the organic nanotubes proved to effectively preserve the anionic GFP via electrostatic attraction, even though both open ends are exposed to the bulk solution. When the pH was increased to 8.9, the fluorescence intensity of GFP at $\lambda = 510$ nm increased whereas the fluorescence intensity Alexa emitted through FRET at $\lambda = 570$ nm decreased (Figure 5, bottom). The reduction in FRET efficiency indicates the release of the encapsulated GFP from the nanochannels to the bulk solution (Figure 6) because the pH of 8.9 induced a dramatic decrease in the electrostatic attraction based on the deprotonation of the amino groups on the inner surface. Addition of Triton X-100 was found to completely destroy the tubular morphologies, and eventually released all the retained GFP in the nanochannels.

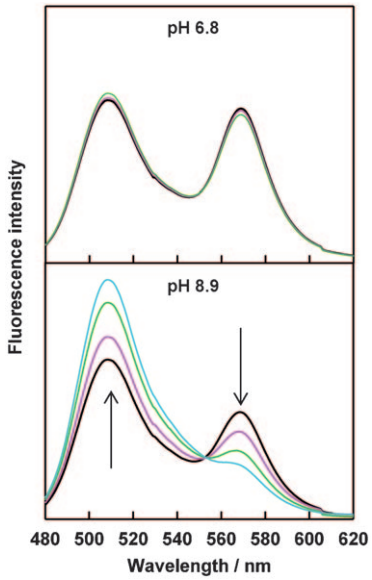

Figure 5. Time dependence of the fluorescence spectra of 20-AlexaNT encapsulating GFP at 25 °C under different pH conditions (——: 0 h, ——: 10 h, ——: 40 h, ——: 80 h). Excitation at $\lambda = 450$ nm.

The release rate of GFP decreased as the inner diameters of the organic nanotubes were decreased. Although the dependence of the release rate on the inner diameter is in accord with that of the above diffusion constant, the release rate was clearly slow compared with the encapsulation rate, which was completed in a few seconds. The percentage of GFP released reached a maximum of 50–60 % before addition of Triton X-100 (Figure 6), which suggests that the driving force for the release is mainly attributable to desorption from the inner nanotube surface covered with a small amount of protonated amino groups. The size and concentration effects of the guests[7,8] and the polarity of solvents surrounding the guests[18] on such dynamic behavior have already been reported. Herein, we have for the first time determined the size effect of tubular nanoarchitectures (meso-

 © 2010 Wiley-VCH Verlag GmbH & Co. KGaA, Weinheim

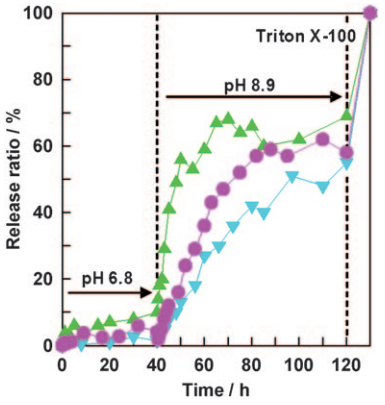

Figure 6. Time and pH dependence of the release rate of GFP from the AlexaNT channels (▲: 80-AlexaNT, ●: 20-AlexaNT, ▼: 10-AlexaNT) at 25 °C under different pH conditions.

scale hosts) on the transportation, diffusion, and release of guest molecules.

Thermal and chemical stabilities of GFP in organic nanotube channels: The fluorescence intensity of GFP sharply responds to denaturation behavior, that is, native GFP fluoresces strongly, whereas it results in nonfluorescence upon denaturation.[19] Elevated temperatures in the range of 20 to 85 °C caused a decrease in the relative fluorescence intensity of free GFP at $\lambda = 510$ nm in the bulk solution (Figure 7). Therefore, thermal denaturation of GFP proceeds slowly on heating. Temperature elevation also caused a decrease in the relative fluorescence at $\lambda = 570$ nm that represents the efficiency of FRET from the encapsulated GFP to the interior Alexa of 80-AlexaNT or 20-AlexaNT. These results suggest that the fluorescence intensity of the encapsulated GFP itself decreases by thermal denaturation. On the other hand, the FRET efficiency from the encapsulated GFP to the Alexa of 10-AlexaNT proved to be insensitive to the elevated temperatures, which indicates that the encapsulated GFP shows no denaturation under given conditions. This temperature dependence of the *endo*-sensing features by using the FRET system clearly shows that the thermal stability of GFP strongly depends on the inner diameters of the organic nanotubes.

We also performed circular dichroism (CD) spectroscopy to directly monitor the denaturation behavior of GFP. Native GFP in a folded state has a strong CD band at around $\lambda = 215$ nm based on a highly ordered conformation, whereas denatured GFP in a defolding state gives a very weak one.[19] In fact, the CD spectra indicate that GFP encapsulated by 10-AlexaNT retained strong CD activity after incubation at 80 °C for 1 day, whereas the CD signal for GFP encapsulated by 20-AlexaNT and 80-AlexaNT and free GFP in the bulk solution is considerably decreased (Figure 8). Figure 9 shows the temperature dependence of the CD intensity at $\lambda = 215$ nm. Thermal denaturation of GFP encapsulated by 80-AlexaNT was comparable with that of free GFP in the bulk solution. The most remarkable de-

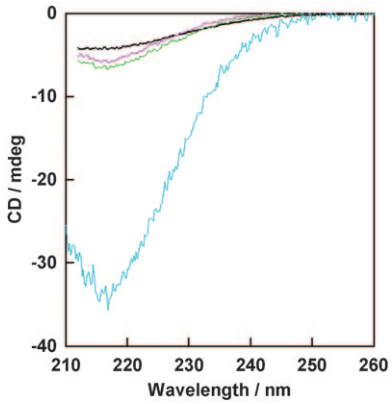

Figure 8. CD spectra of GFP encapsulated in AlexaNT channels (——: 80-AlexaNT, ——: 20-AlexaNT, ——: 10-AlexaNT) and free GFP (——) after incubation at 80 °C for 24 h.

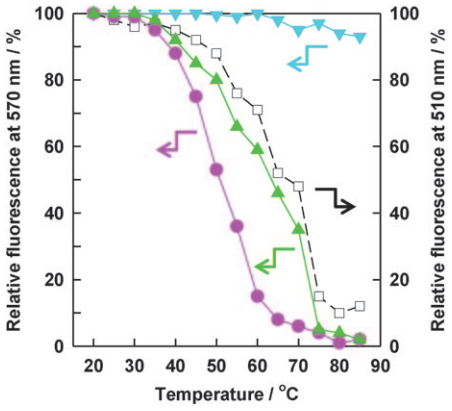

Figure 7. Thermal stability of GFP encapsulated in AlexaNT channels (▲: 80-AlexaNT, ●: 20-AlexaNT, ▼: 10-AlexaNT) and free GFP (□) at pH 6.8. The samples were incubated for 24 h after the temperature was elevated to a particular level. The fluorescence intensities at $\lambda = 510$ and 570 nm were utilized in the calculation of the relative fluorescence [%] for encapsulated GFP and free GFP, respectively.

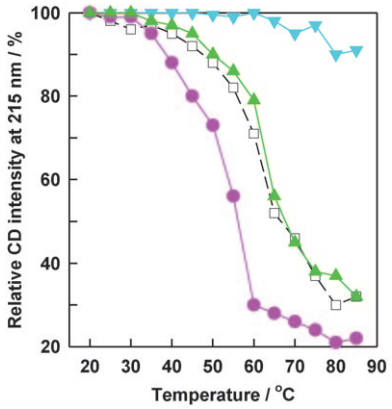

Figure 9. Thermal stability of GFP encapsulated in AlexaNT channels (▲: 80-AlexaNT, ●: 20-AlexaNT, ▼: 10-AlexaNT) and free GFP (□) at pH 6.8. The samples were incubated for 24 h after the temperature was elevated to a particular level.

 © 2010 Wiley-VCH Verlag GmbH & Co. KGaA, Weinheim

naturation was observed for GFP encapsulated by 20-AlexaNT, whereas GFP in 10-AlexaNT showed no denaturation.

Addition of urea as a nonionic denaturant to free GFP in the bulk solution caused a decrease in the relative fluorescence and the CD intensity, which indicates that the GFP was chemically denatured (Figure 10). On the other hand, the inner diameters of the nanochannels significantly influenced the chemical denaturation of GFP encapsulated in organic nanotubes by urea. At high concentrations ($\approx$6 mol L^{-1}), the nonionic urea was able to penetrate the nanochannels through a concentration gradient. About 90% of GFP encapsulated in 10-AlexaNT remained in the native state despite the coexistence of sufficient urea to induce denaturation in the nanochannel.

The influence of the inner diameter on the chemical stability shows similar features to that of the thermal stability (Figures 9 and 10). GFP encapsulated in the 10 nm nanochannel, which is closest to the size of GFP (3×4 nm), showed the strongest resistance to heating and denaturant action. The 80 nm nanochannel was so large that the denaturation of encapsulated GFP was comparable with that of free GFP in the bulk solution. Tightly restricted nanochannel geometry kinetically and thermodynamically prevents the denaturation of GFP. The 20 nm nanochannel, which has loose geometry in terms of GFP, accelerated the denaturation of the encapsulated GFP. Similar confinement effects on denaturation resistance have been reported for various proteins encapsulated in mesoporous silica,[20,21] although to date the mechanism has not yet been clarified.

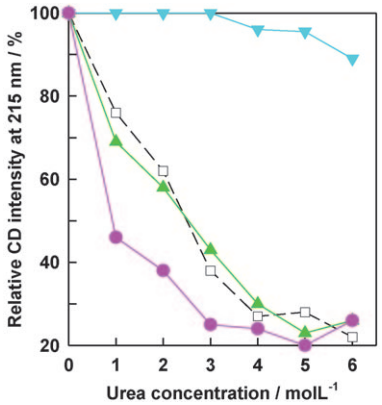

Figure 10. Chemical stability of GFP encapsulated in AlexaNT channels (▲: 80-AlexaNT, ●: 20-AlexaNT, ▼: 10-AlexaNT) and free GFP (□) at pH 6.8. The incubation time after addition of urea was 1 h.

We have already demonstrated that water confined in a 10 nm organic nanotube channel, the inner and outer surfaces of which are covered with identical glucose headgroups, possesses a relatively higher viscosity and lower polarity as compared with bulk water.[22] More recently, we characterized water confined in the present 10 nm organic nanotube by using time-resolved fluorescence spectroscopy.[23] The results show that the change in the physical properties of the confined water is slightly smaller than that in the previous study. These characteristics of water confined in the 10 nm nanochannel should stabilize the hydration structure of GFP even though urea is known to denature GFP through effective destruction of the hydration structure. The physical properties of the confined water depend on the distance from the surface of a nanochannel shaped by a fused-silica microtip[24] and the size of the nanochannel and nanopillar.[25] Therefore, the contribution of this stabilization due to the water in the 20 and 80 nm nanochannels should be much smaller than that of the water in the 10 nm nanochannel.

Conclusion

We have clarified for the first time the dynamic behavior and stabilities of GFP encapsulated in organic nanotube channels with different inner diameters by using a FRET system between a sensing probe immobilized on the inner surface of the nanotube and a protein. Information about the effect of the inner diameter on the diffusion constant and release rate of the encapsulated GFP is very important for constructing novel nanocontainers for drug-delivery systems. The organic nanotubes show a remarkable confinement effect that stabilizes the encapsulated protein under thermally and chemically unfavorable conditions. Therefore, they are also able to act as a novel soft material that is widely applicable to biological and medical fields.

Experimental Section

Immobilization of Alexa in the organic nanotubes: The 80 nm organic nanotube (10 mg, lipid: 18 μmol) self-assembled from *N*-(2-aminoethyl)-*N'*-(β-D-glucopyranosyl)icosanediamide **1**[5] was mixed with Alexa Fluor 546 carboxylic acid succinimidyl ester (Alexa-OSu, 10 μmol; Molecular Probes) in water (100 mL) at pH 10, adjusted by NaOH. The mixed solution was stirred at 60 °C for 24 h and then cooled to RT. Unreacted Alexa-OSu was completely removed by using a polycarbonate membrane filter with 200 nm pore size. The organic nanotubes were easily collected on the membrane because of their high axial ratio structures. Fluorescence spectroscopy indicated that 1.2 μmol of Alexa participates in the reaction with the amino groups of **1** (see the Supporting Information). Because the organic nanotube consists of two stacking layers, less than 9 μmol of the amino groups (half of the total lipid) are located on the inner surface. Therefore, the percentage of Alexa immobilized on the amino groups on the inner surface was estimated to be about 13% (100×(1.2 μmol/9 μmol)). Immobilization of Alexa (9 μmol) in the 20 nm organic nanotube (10 mg, lipid: 18 μmol) self-assembled from **1**[9] was performed by the same manner as above. Fluorescence spectroscopy indicated that 1.0 μmol of Alexa binds to the amino groups (less than 9 μmol) on the inner surface. The immobilization percentage was about 11%. 10-AlexaNT was prepared by adding Alexa-OSu (10 μmol) to a weakly acidic (pH 4) aqueous solution of *N*-(β-D-glucopyranosyl)-*N'*-(2-glycylglycylglycineamideethyl)octadecane diamide **3** (7 mg, 10 μmol). Addition of NaOH to adjust the mixed solution to pH 10 gave 10 nm organic nanotubes.[11] The aqueous dispersed solution was heated to 60 °C for 24 h and then cooled to RT. Unreacted Alexa-OSu was removed by using the filtration procedure above. Fluorescence spectroscopy indicated that 1.8 μmol of Alexa participates in the reaction with the amino groups of **3** (see the Supporting Information). Because the organic nanotube consists of a monolayer, all amino groups are located on the inner surface. There-

 © 2010 Wiley-VCH Verlag GmbH & Co. KGaA, Weinheim

fore, the percentage of Alexa immobilized on the amino groups on the inner surface was estimated to be about 18% (100×(1.8 μmol/10 μmol)).

Time-lapse fluorescence microscopy: Time-lapse fluorescence microscopic observation for the Alexa-immobilized nanotubes after addition of GFP was carried out by using an inverted microscope (Olympus IX71) equipped with a CCD camera (Hamamatsu ORCA-ER). The excitation optical source consisted of a high-pressure mercury lamp (100 W, Olympus BH2-REL-T3). Time-lapse fluorescence microscopic images for the FRET phenomenon were recorded on a PC by using an Aquacosmos system (Hamamatsu). The measurement interval was set to 50–100 ms.

Preparation of GFP-encapsulating Alexa-immobilized nanotubes: Encapsulation was performed by mixing an aqueous solution of GFP (0.5 mg mL^{-1}, 20 mmol L^{-1} Tris-HCl buffer) and an aqueous dispersion containing Alexa-immobilized nanotubes (1–2 mg mL^{-1}) at 25°C. The pH of the solution was adjusted to 6.8 by using HCl and NaOH, then the mixture was filtered through a polycarbonate membrane with a pore size of 200 nm. The residue of the GFP-encapsulating Alexa-immobilized nanotubes was washed several times to remove free, unencapsulated GFP while maintaining a pH of 6.8. To estimate the amount of encapsulated GFP, the resultant nanotubes were destroyed by addition of 5% Triton X-100. The amount of forcibly released GFP, which corresponds to the total amount, was calculated to be 19, 15, and 22 mg mL^{-1} for 10-AlexaNT, 20-AlexaNT, and 80-AlexaNT, respectively, by fluorescence spectroscopy at the fluorescence intensity of GFP at $\lambda = 510$ nm.

Release experiment: The release of GFP was monitored after allowing the GFP-encapsulating Alexa-immobilized nanotubes to stand in water at pH 6.8 and 8.9. The percentage of GFP released over time was calculated by the following equation: Release (%) $= 100 \times F_{release}(t)/F_{total}$. $F_{release}(t)$ was evaluated each time, and is the fluorescence intensity of GFP released into the bulk solution at a certain time *t*. F_{total} is the fluorescence intensity of the total amount of encapsulated GFP as described above. In the release experiments, we never observed a loss of fluorescence due to denaturation of GFP under the given conditions (pH, standing time, and addition of detergent) at RT.

Evaluation of thermal and chemical stabilities: Aqueous dispersions of GFP only or GFP encapsulated by Alex-immobilized nanotubes were heated to 25–85°C for 24 h at pH 6.8. Each solution was rapidly cooled to room temperature and subjected to fluorescence and CD spectroscopies. The relative fluorescence intensity (%) was calculated from the ratio of the fluorescence intensity, F_{after}/F_{before}, in which F_{after} and F_{before} are the fluorescence intensity of the free GFP at $\lambda = 510$ nm and the Alexa via FRET at $\lambda = 570$ nm after and before heating, respectively. The relative CD intensity (%) was calculated from the ratio of the CD intensity of the free GFP or the encapsulated GFP at $\lambda = 215$ nm after and before heating. Urea (1–6 mol L^{-1}), used as a nonionic denaturant, was added into the aqueous dispersions of GFP only or GFP encapsulated by Alexa-immobilized nanotubes. Each solution was allowed to stand at 25°C for 1 h before being analyzed by using fluorescence and CD spectroscopies.

Acknowledgements

This work was partly supported by a Grant-in-Aid for Young Scientists (B) (no. 21710117) from the Ministry of Education, Culture, Sports, Science and Technology (MEXT).

[1] For a review, see: T. Shimizu, M. Masuda, H. Minamikawa, *Chem. Rev.* **2005**, *105*, 1401–1443.

[2] For reviews, see: a) X. Gao, H. Matsui, *Adv. Mater.* **2005**, *17*, 2037–2050; b) Y. Zhou, T. Shimizu, *Chem. Mater.* **2008**, *20*, 625–633.

[3] For reviews, see: a) T. Shimizu, *J. Polym. Sci. Part A* **2006**, *44*, 5137–5152; b) T. Shimizu, *J. Polym. Sci. Part A* **2008**, *46*, 2601–2611.

[4] For bio-applications, see: a) J. M. Schnur, R. Price, A. S. Rudolph, *J. Controlled Release* **1994**, *28*, 3–13; b) A. S. Goldstein, M. H. Gelb, P. Yager, *J. Controlled Release* **2001**, *70*, 125–138; c) S. M. Nomura, Y. Mizutani, K. Kurita, A. Watanabe, K. Akiyoshi, *Biochim. Biophys. Acta Biomembr.* **2005**, *1669*, 164–169; d) L. Yu, I. A. Banerjee, X. Gao, N. Nuraje, H. Matsui, *Bioconjugate Chem.* **2005**, *16*, 1484–1487; e) U. Raviv, D. J. Needleman, C. R. Safinya, *J. Phys. Condens. Matter* **2006**, *18*, S1271–S1279; f) J. Hurtig, O. Orwar, *Soft Matter* **2008**, *4*, 1515–1520; g) P. K. Vemula, G. John, *ACC. Chem. Res.* **2008**, *41*, 769–782.

[5] N. Kameta, M. Masuda, H. Minamikawa, N. V. Goutev, J. A. Rim, J. H. Jung, T. Shimizu, *Adv. Mater.* **2005**, *17*, 2732–2736.

[6] N. Kameta, H. Minamikawa, M. Masuda, G. Mizuno, T. Shimizu, *Soft Matter* **2008**, *4*, 1681–1687.

[7] N. J. Meilander, X. Yu, N. P. Ziats, R. V. Bellamkonda, *J. Controlled Release* **2001**, *71*, 141–152.

[8] L. Guo, P. Chowdhury, J. Fang, F. Gai, *J. Phys. Chem. B* **2007**, *111*, 14244–14249.

[9] N. Kameta, M. Masuda, H. Minamikawa, Y. Mishima, I. Yamashita, T. Shimizu, *Chem. Mater.* **2007**, *19*, 3553–3560.

[10] N. Kameta, M. Masuda, G. Mizuno, N. Morii, T. Shimizu, *Small* **2008**, *4*, 561–565.

[11] N. Kameta, K. Yoshida, M. Masuda, T. Shimizu, *Chem. Mater.* **2009**, *21*, 5892–5898.

[12] G. M. Barrow, *Physical Chemistry*, 5th ed., McGraw-Hill, New York, **1988**.

[13] R. Karlsson, M. Karlsson, A. Karlsson, A. S. Cans, J. Bergenholtz, B. Akerman, A. G. Ewing, M. Voinova, O. Orwar, *Langmuir* **2002**, *18*, 4186–4190.

[14] H. Brenner, L. J. Gaydos, *J. Colloid Interface Sci.* **1977**, *58*, 312–356.

[15] a) W. M. Deen, *AIChE J.* **1987**, *33*, 1409–1425; b) H. Yoshida, M. Yoshikawa, T. Kataoka, *AIChE J.* **1994**, *40*, 2034–2044; c) J. Li, F. F. Cantwell, *J. Chromatogr. A* **1996**, *726*, 37–44; d) K. Miyabe, G. Guiochon, *Anal. Chem.* **2000**, *72*, 1475–1489.

[16] a) K. Nakatani, T. Sekine, *Langmuir* **2000**, *16*, 9256–9260; b) K. Chikama, H. Kakizaki, K. Nakatani, *Colloids Surf. A* **2008**, *315*, 250–253.

[17] T. Sekine, K. Nakatani, *Chem. Lett.* **2004**, *33*, 600–601.

[18] a) K. Okamoto, C. J. Shook, L. Bivona, S. B. Lee, D. S. English, *Nano Lett.* **2004**, *4*, 233–239; b) K. Jayaraman, K. Okamoto, S. J. Son, C. Luckett, A. H. Gopalani, S. B. Lee, D. S. English, *J. Am. Chem. Soc.* **2005**, *127*, 17385–17392.

[19] M. Chalfie, S. R. Kain, *Green Fluorescent Protein: Properties, Applications, and Protocols*, Wiley-Interscience, New York, **2006**.

[20] For a review, see: S. Hudson, J. Cooney, E. Magner, *Angew. Chem.* **2008**, *120*, 8710–8723; *Angew. Chem. Int. Ed.* **2008**, *47*, 8582–8594.

[21] a) Y. Urabe, T. Shiomi, T. Itoh, A. Kawai, T. Tsunoda, F. Mizukami, K. Sakaguchi, *ChemBioChem* **2007**, *8*, 668–674; b) H. H. P. Yiu, P. A. Wright, *J. Mater. Chem.* **2005**, *15*, 3690–3700; c) B. Campanini, S. Bologna, F. Cannone, G. Chirico, A. Mozzarelli, S. Bettati, *Protein Sci.* **2005**, *14*, 1125–1133.

[22] H. Yui, Y. Guo, K. Koyama, T. Sawada, G. John, B. Yang, M. Masuda, T. Shimizu, *Langmuir* **2005**, *21*, 721–727.

[23] Unpublished data.

[24] a) A. Hibara, T. Saito, H.-B. Kim, M. Tokeshi, T. Ooi, M. Nakano, T. Kitamori, *Anal. Chem.* **2002**, *74*, 6170–6176; b) T. Tsukahara, A. Hibara, Y. Ikeda, T. Kitamori, *Angew. Chem.* **2007**, *119*, 1199–1202; *Angew. Chem. Int. Ed.* **2007**, *46*, 1180–1183.

[25] N. Kaji, R. Ogawa, A. Oki, Y. Horiike, M. Tokeshi, Y. Baba, *Anal. Bioanal. Chem.* **2006**, *386*, 759–764.

Received: December 14, 2009
Published online: March 16, 2010

 © 2010 Wiley-VCH Verlag GmbH & Co. KGaA, Weinheim